ISPRS Journal of Photogrammetry and Remote Sensing 164 (2020) 11–25

Contents lists available at ScienceDirect

ISPRS Journal of Photogrammetry and Remote Sensing

journal homepage: www.elsevier.com/locate/isprsjprs

National wetland mapping in China: A new product resulting from object-based and hierarchical classification of Landsat 8 OLI images

Dehua Mao[a], Zongming Wang[a,e,*], Baojia Du[a], Lin Li[b], Yanlin Tian[a], Mingming Jia[a], Yuan Zeng[c], Kaishan Song[a], Ming Jiang[a], Yeqiao Wang[d,*]

[a] Key Laboratory of Wetland Ecology and Environment, Northeast Institute of Geography and Agroecology, Chinese Academy of Sciences, Changchun 130102, Jilin, China
[b] Department of Earth Sciences, Indiana University-Purdue University, Indianapolis 46202, IN, USA
[c] Aerospace Information Research Institute, Chinese Academy of Sciences, Beijing 100094, China
[d] Department of Natural Resources Sciences, University of Rhode Island, Kingston, RI 02881, USA
[e] National Earth System Science Data Center, Beijing 100101, China

ARTICLE INFO

Keywords:
Wetland mapping
Landsat 8 OLI
Object-based
CAS_Wetlands
China

ABSTRACT

Spatially and thematically explicit information of wetlands is important to understanding ecosystem functions and services, as well as for establishment of management policy and implementation. However, accurate wetland mapping is limited due to lacking an operational classification system and an effective classification approach at a large scale. This study was aimed to map wetlands in China by developing a hybrid object-based and hierarchical classification approach (HOHC) and a new wetland classification system for remote sensing. Application of the hybrid approach and the wetland classification system to Landsat 8 Operational Land Imager data resulted in a wetland map of China with an overall classification accuracy of 95.1%. This national scale wetland map, so named CAS_Wetlands, reveals that China's wetland area is estimated to be 451,084 ± 2014 km^2, of which 70.5% is accounted by inland wetlands. Of the 14 sub-categories, inland marsh has the largest area (152,429 ± 373 km^2), while coastal swamp has the smallest coverage (259 ± 15 km^2). Geospatial variations in wetland areas at multiple scales indicate that China's wetlands mostly present in Tibet, Qinghai, Inner Mongolia, Heilongjiang, and Xinjiang Provinces. This new map provides a new baseline data to establish multi-temporal and continuous datasets for China's wetlands and biodiversity conservation.

1. Introduction

Wetlands perform a variety of functions and provide multiple ecosystem services, which are critical to biodiversity, ecological security, and human well-being (MA, 2005, Wang et al., 2012). During the past few decades, wetlands worldwide have been declined and degraded dramatically due to enhanced human activities and climatic changes (Asselen et al., 2013). Such deteriorations of wetland environment have caused evident ecological consequences including biodiversity loss, habitat fragmentation, floods, and droughts (Kirwan and Megonigal, 2013; Mao et al., 2018a). Accurate and up-to-date information on the spatial distribution of wetlands is essential for improving our understanding about ecosystem conditions and management implementations, such as biodiversity conservation, habitat assessment, and quantification of biogeochemical cycles and spatial patterns (Nahlik & Fennessy, 2016; Zhu & Gong, 2014; Zhu et al., 2015).

China has extensive coverage of wetlands and also experienced a striking wetland loss (Gong et al., 2010; Mao et al., 2018b; Niu et al., 2012). Important values and remarkable loss of wetlands in China have drawn attention from academia, governmental agencies, and land and resource managers (Mao et al., 2019a). Scarcity of spatially explicit wetland extent and distribution across the country imposes a strong limitation to policy making and implementation for ecosystem conservation. Meanwhile, such data deficiency makes it difficult to evaluate wetlands for their habitat health, carbon storage and greenhouse gas emission, and ecosystem service capacity in China. Chinese government launched two national wetland inventories (NWIs) from 1995 to 2003 and from 2009 to 2014. Chinese Academy of Sciences (CAS) first mapped China's vegetated wetlands at the national scale in 1995 using traditional cartography and field survey. The achieved hard copy maps at 1: 4,000,000, however, might not be applicable toward practical usage in wetland management and investigations (Yan et al.,

* Corresponding authors at: Key Laboratory of Wetland Ecology and Environment, Northeast Institute of Geography and Agroecology, Chinese Academy of Sciences, Changchun 130102, Jilin, China (Z. Wang).
E-mail addresses: zongmingwang@iga.ac.cn (Z. Wang), yqwang@uri.edu (Y. Wang).

https://doi.org/10.1016/j.isprsjprs.2020.03.020
Received 19 September 2019; Received in revised form 4 March 2020; Accepted 30 March 2020
Available online 09 April 2020

2017). A digital wetland map of China has been produced and included in the China Land Use Database (CLUD, Liu et al., 2014) and the China National Land Cover Database (ChinaCover, Mao et al., 2018a). However, these maps lack details on wetland categories. Niu et al. (2009) made the first attempt to map China's wetlands in detail with almost 600 Landsat Enhanced Thematic Mapper plus (ETM +) images acquired from 1999 to 2002, and classified wetlands into 3 categories and 14 sub-categories based on the *Ramsar* wetland definition. Gong et al. (2010) mapped China's wetland change from 1990 to 2000 using Landsat Thematic Mapper (TM) images. Nevertheless, these mapping results and accuracies had limitations due to the data source quality and classification. Developing more accurate wetland maps has continued to be a challenge and is urgently needed in China.

Recently reported local or regional studies on mapping wetlands worldwide with remote sensing are devoted to alpine lakes on the Tibetan Plateau of China (Mao et al., 2018c), coastal aquaculture ponds in India (Prasad, et al., 2019), salt marshes along the mid-Atlantic coast of the United States (Campbell and Wang, 2019, 2020), and mangrove swamps in the Campeche of Mexico (Cissell et al., 2018). Due to differences in geographic locations and wetland types, reported studies revealed that suitable method should be selected to delineate various wetland categories (Adam et al., 2010). Many machine learning algorithms including supervised classification, support vector machines (SVM), random forest (RF), and deep learning had achieved rapid mapping of worldwide wetlands (Amani et al., 2019a; Mahdavi et al., 2017; Rezaee et al., 2018). However, most of those studies were based on pixel-based classification that is affected by wetland complexity and relies on a large number of ground truth samples (Gallant, 2015; Mui et al., 2015; Zhang et al., 2014). Moreover, landscape features, such as shape and texture, which are important to improve classification accuracy, could not be utilized to identify wetlands (Dronova, 2015). Object-based image analysis (OBIA) can delineate satellite images into homogeneous objects (Blaschke, 2010), allows to use locally different decision-rules to classify wetlands, can integrate different types of complementary datasets to improve wetland mapping (Dronova, 2015), and has been adopted in several recent wetland mapping studies (Campbell and Wang, 2018; Dronova et al., 2011; Mao et al., 2018c). However, most of existing studies have been performed in small spatial scales (Campbell and Wang, 2019; Dronova et al., 2011; Kloiber et al., 2015). Application of OBIA to map wetlands accurately at a large scale needs to be explored.

Multi-source remote sensing data including optical, hyperspectral, and SAR images have been used to identify worldwide wetlands (Guo et al., 2017; Rapinel et al., 2019; Wohlfart et al., 2018). Landsat images have been widely used due to the broad and long term coverage, fine resolution, and free availability (Amani et al., 2019b, Mao et al., 2019b). Landsat data archives provide global images with a resolution of 30/80 m to establish consistent dataset for documenting historical wetland changes from 1970s to very recent. The new sensor, Landsat-8 Operational Land Imager (OLI), can acquire multi-temporal images at improved quality and capacity compared to previous Landsat sensors (Roy et al., 2014), which have been used for mapping wetland categories at large scales. OLI applications have been typified by mapping paddy rice fields in northeastern Asia (Dong et al., 2016), lake water extent in Oceania (Sheng et al., 2016), mangroves (Jia et al., 2018), *Spartina alterniflora* (Liu et al., 2018), and tidal flats (Wang et al., 2020) in coastal China.

The primary objective of this study is to produce a wetland map of China with OLI data. Building upon the potential of medium resolution satellite images for classifying different wetland categories and the ecological definition of wetland, we developed a remote sensing classification system and a hybrid object-based and hierarchical classification approach for wetland mapping. Specifically, the objectives of this study are to (1) improve the area estimation of wetland and its composition, (2) document the up-to-date pattern of various wetland categories in China and examine their geospatial variations.

2. Materials and methods

2.1. Wetland classification system for remote sensing

The Ramsar definition of wetlands include areas of marsh, fen, peatland, and water, whether natural or artificial, permanent or temporary, and whether water is static or flowing, fresh, brackish or salty, including areas of marine water the depth of which at low tide does not exceed 6 m (Gong et al., 2010). This definition is widely accepted due to its comprehensive consideration on the features of global wetlands. Referring to this definition and an unprecedented amount of field samples in the wetland mapping history of China, the developed remote sensing wetland classification system considers the applicability of moderate resolution images and its practical use for ecosystem management. Therefore, one of the novelties of this study is the creation of a new wetland classification system. In the classification system, wetlands are grouped into 3 broad categories and 14 sub-categories (Table 1). Although it is an important human-made wetland category, paddy field was excluded from our classification because it is more appropriate for it to be categorized as farmland. Floodplain was not categorized to an individual class because it can be included in other wetland categories such as river and marsh in wet season.

2.2. Satellite images and data preprocessing

Landsat OLI images were downloaded from the United States Geological Survey (USGS) and the Internal Scientific Data Service Platform of China (ISDP) websites. Altogether, 546 scenes of OLI images with paths from 113 to 151 and rows from 23 to 57 are needed to cover the entire land area of China. Initially, 2437 OLI images with cloud cover less than 5% were collected in 2015. However, some of the areas in southern China were covered insufficiently or even less in 2015 (Fig. 1A). Therefore, selected were OLI images in 2014 and 2016 with cloud cover less than 5%, and in 2015 with cloud cover between 5% and 10% (Fig. 1B) to ensure that at least two images cover each task block. Finally, 1436 OLI images were used for wetland classification, and the images were mostly acquired during the growing season (March to October) besides the images acquired in winter for southern China (Fig. 1C).

Landsat 8 OLI images possess 9 spectral bands with a spatial resolution of 30 m except the panchromatic band (band 8) at a spatial resolution of 15 m. Prior to wetland extraction, image preprocessing including geometric, topographic, and radiometric corrections was performed for all the images using the ENVI 5.1 software package. The classification was divided into task blocks to ensure the classification efficiency (Fig. 1D). The Shuttle Radar Topography Mission (SRTM) digital elevation model (DEM) with a spatial resolution of 30 m was downloaded and merged to cover the entire mapped area. The slope gradient layer was generated from DEM using the software ArcGIS (version 9.3).

2.3. Acquisition of training and validating samples

The training and validating samples were obtained through field investigation, national research projects, published literatures, and public databases (Fig. 2). The field surveys were carried out from June 2014 to September 2016, in which wetland categories were recorded for their locations using a hand-held geographic positioning systems (GPS) with error smaller than 2 m connected to a laptop and photographed using a digital camera. Interviews with local people were also performed to collect data on historical distributions of wetlands. Unmanned aerial vehicles (UAV) equipped with a real-time kinematic (RTK) GPS were used to identify the categories of those inaccessible wetlands. Moreover, some inaccessible wetlands were determined by interpreting high-resolution satellite images (e.g. SPOT with a resolution of 6 m and Chinese GF-2 with a resolution of 8 m) and Google Earth

Table 1
Wetland classification system for remote sensing.

Category I	Category II	Description	OLI image example	Field photo example
Inland wetland	Inland swamp	Natural wetland with dominant woody vegetation in inland areas including forested wetland and shrub wetland	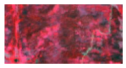	
	Inland marsh	Natural wetland with dominant herbaceous vegetation in inland areas		
	Lake	Natural polygon waterbody with standing water in inland areas		
	River	Natural linear waterbody with flowing water in inland areas		
Coastal wetland	Coastal swamp	Natural wetland with dominant woody vegetation in coastal areas including forested wetland and shrub wetland		
	Coastal marsh	Natural wetland with dominant herbaceous vegetation in coastal areas		
	Lagoon	Shallow polygon waterbody separated from sea by barrier islands or reefs and with at least one relatively narrow connection to the sea		
	Estuarine water	Natural linear waterbody with flowing water from the boundary of inland areas to coastline	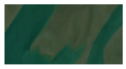	
	Tidal flat	The intertidal flat with no or very low vegetation coverage including sand beach, rocky shore, and coral reef	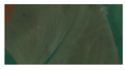	
	Shallow marine water	Marine waterbody between coastline and the contour of 6-m depth		
Human-made wetland	Reservoir/pond	Artificial polygon waterbody with standing water generally with obvious dam	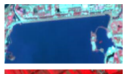	
	Canal/channel	Artificial linear waterbody with flowing water generally with obvious dam or straight boundary		
	Salt pan	Artificial flat depression ground covered with salt and other minerals close to sea		
	Aquaculture pond	Polygon waterbody used for aquaculture with regular shape and close to river or sea		

images. There were time inconsistencies between field surveys and Landsat-8 image acquisitions. However, the influence of probable land use change could be neglected because the geographical locations for all the field samples were recorded for permanent wetlands.

Two national projects funded by the Ministry of Science and Technology of China investigated numerous wetlands in China. The 3325 wetland sites identified by the two projects were used in this study. In addition, 4578 field sites labelled as lakes and reservoirs (Ma et al., 2011; Song et al., 2018) and coastal wetlands (Jia et al., 2018; Mao et al., 2019b) determined by previous studies were adopted as the reference samples in this study.

In total, 16,496 effective ground reference samples representing various wetland categories were selected for seven geographic regions (Fig. 2). Of which, 11,474 samples were used in training classification rules and dataset improvement, and 5022 samples (approximately 30% of the total samples) randomly selected for all wetland categories were used for validation of the classification result.

2.4. A hybrid object-based and hierarchical classification approach (HOHC)

To achieve an accurate wetland mapping, a hybrid approach integrating OBIA and decision-tree classification was used in this study. Detailed components are described as follows:

2.4.1. Object-based and hierarchical classification

Object-based image analysis was performed using the eCognition version 9.2 because the approach has its advantages in delineating object boundaries and reducing "salt and pepper" effects (Dronova et al., 2011; Zhang et al., 2014). Fig. 3 illustrates a flow chart for object-based and a hierarchical decision-tree chart for delineating different wetland categories. Hierarchical classification trees were designed based on the wetland classification system, and of which various classification rules constituted by spectral, landscape, and environmental features were tested to identify different wetland categories in different geographic regions.

(1) Multi-resolution segmentation

Multiscale segmentation is an important step to generate homogeneous landscape objects. The OLI bands 1–7 were used in segmentation and their weights were set to 1. In terms of obvious terrain variations and wetland distribution across the country, especially in mountainous areas, terrain slope was considered as a thematic layer in the segmentation process. The normalized difference vegetation index (NDVI) and normalized difference water index (NDWI) are the most widely used in delineating wetlands and thus both indices were input as thematic layers. The segmentation process is based on three parameters, i.e., scale, shape, and compactness for delineating wetland boundaries with Landsat images (Mui et al., 2015).

In this process, segmentation scale primarily controls the accuracy

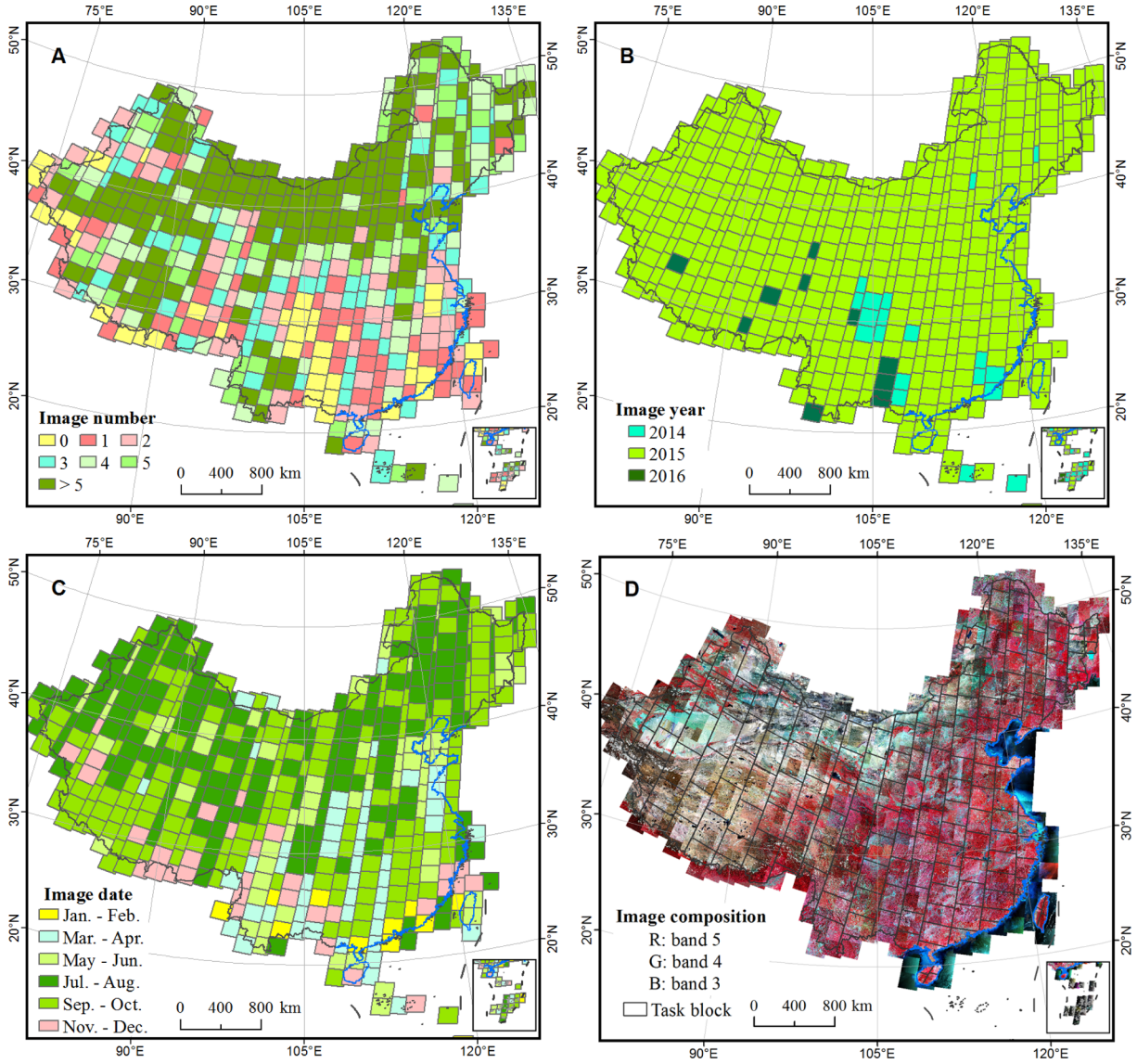

Fig. 1. Landsat 8 OLI image acquisition covering China. A: the number of images with cloud less than 5% for each grid (Path/row) in 2015; B: the distribution of images in adjacent years (2014 and 2016) used for object identification; C: the date for selected images used for classification; D: mosaicked images with standard false color and task blocks for wetland delineation.

of wetland maps and workloads as shown in Fig. 4, in which segmentation with smaller scales generated superfluous information, while segmentation with larger scales yielded imprecise wetland boundaries. Referencing to the polygon objects hand-digitized based on the field samples and images, visual examination (i.e. boundary and area) of the segmented results for different segmentation scales was carried out to determine the optimal scale for landscape features in each task block. As what we tested, landscape complexity determines the range of scale values. In general, homogenous features and patches require to use larger scales with values ranging from 100 to 500, while fragmented landscape needs smaller scales from 10 to 100 to determine the object of interests. Different scale intervals (i.e. 5, 10, and 50) were thus set for the images with different landscape complexities. As stated by Möller et al. (2007) and Mui et al. (2015), several quantitative and automated methods can be used to select the scale parameter, but no algorithms are suitable for all images covering a broad region. Therefore, a semi-automated approach to determining optimal scales would be ideal for improving work efficiency and more repeatable and accessible for researchers. Composition of homogeneity criteria is determined by two indices including shape and compactness. We adopted 0.1 or 0.2 as the coefficient for shape index which controls the object boundary. A value of 0.5 was mostly used for compactness which characterizes the compactness of segmented objects.

(2) Extracting wetlands based on hierarchical decision trees and heterogeneous rulesets

Fig. 5 shows that various wetland categories and other land cover types are spectrally differentiable through calculating multiple spectral indices such as NDVI and NDWI. However, spectral similarity exists among some wetland categories and such spectral similarity yields large uncertainty in delineation of various wetland categories. Due to a large extent of the study area, the landscape complexity requires heterogeneous rulesets. Therefore, spectral (band and indices), landscape (image color, object texture, patch shape, and phenology) and environmental features (e.g., terrain conditions and wetland object location) were jointly used in designing the hierarchical classification tree and heterogeneous rulesets (Table 2). Samples in different geographic regions were respectively trained for the corresponding wetland classification. In each task block, all the selected spectral indices (Table 2)

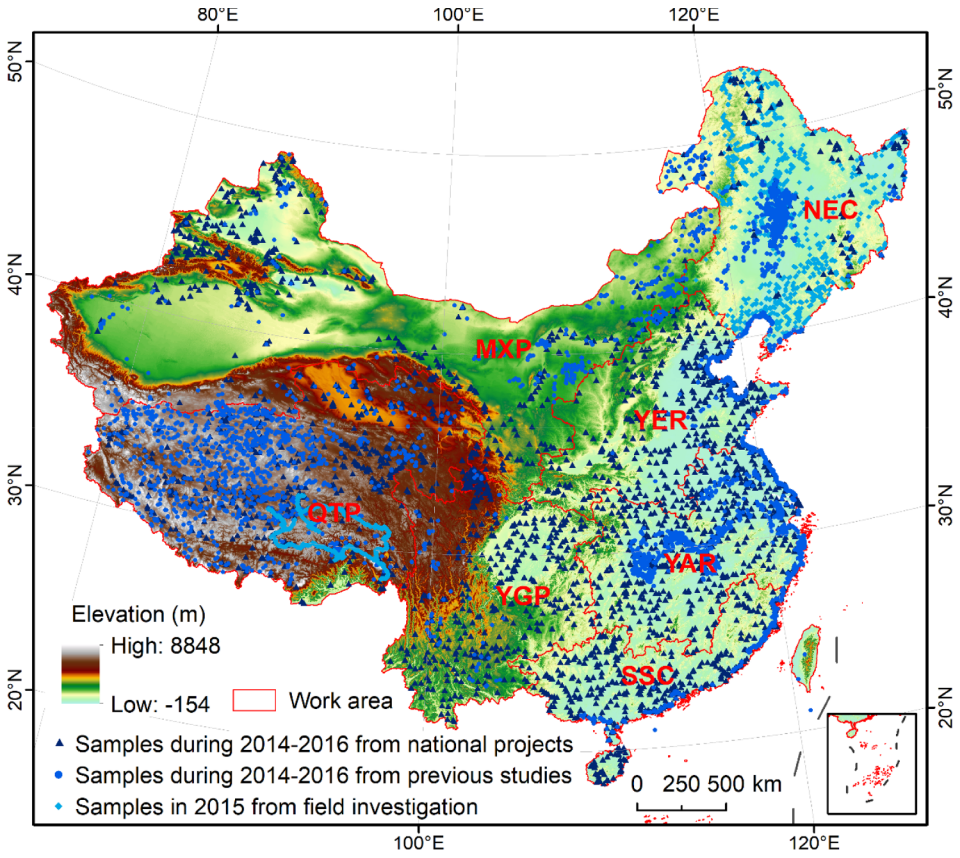

Fig. 2. Locations of wetland field samples over different work areas, i.e. NEC: Northeast China; MXP: Inner Mongolia-Xinjiang Plateau; YER: lower and middle reaches of Yellow River; QTP: Qinghai-Tibet Plateau; YAR: lower and middle reaches of Yangtze River; YGP: Yunnan-Guizhou Plateau; SSC: Southeast and South China. The background indicates the terrain variations among these work areas.

were calculated. A statistical analysis for the segmented objects, field samples located in, was performed to obtain the referencing thresholds for wetland interpretation. The referencing thresholds of various spectral indices in adjacent blocks were used when necessary.

As specified in Fig. 3B, spectral indices were needed at different classification nodes. Water spectral signal is the most important feature for wetlands and thus water-related indices were used in our classification. Different NDWI thresholds were tested for different blocks to distinguish the wetlands. Although NDWI is effective in distinguishing wetlands in arid zones, it is not an optimal index for urban and mountain areas because shadows casted by mountains or by high buildings in most cities can lead to wetland misclassification (Pekel et al., 2016). Therefore, NDWI combined with terrain slope and normalized difference snow index (NDSI) was used to extract alpine

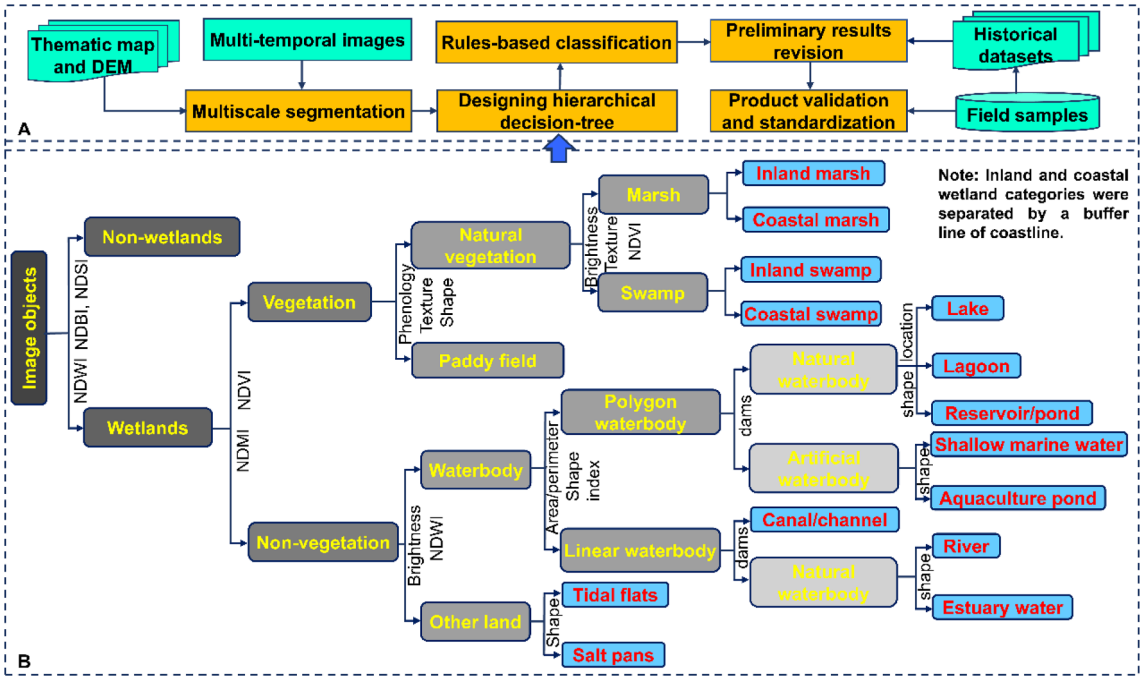

Fig. 3. A general description of HOHC. A: classification flow chart; B: hierarchical decision-tree; the classification was like that black box was gradually opened.

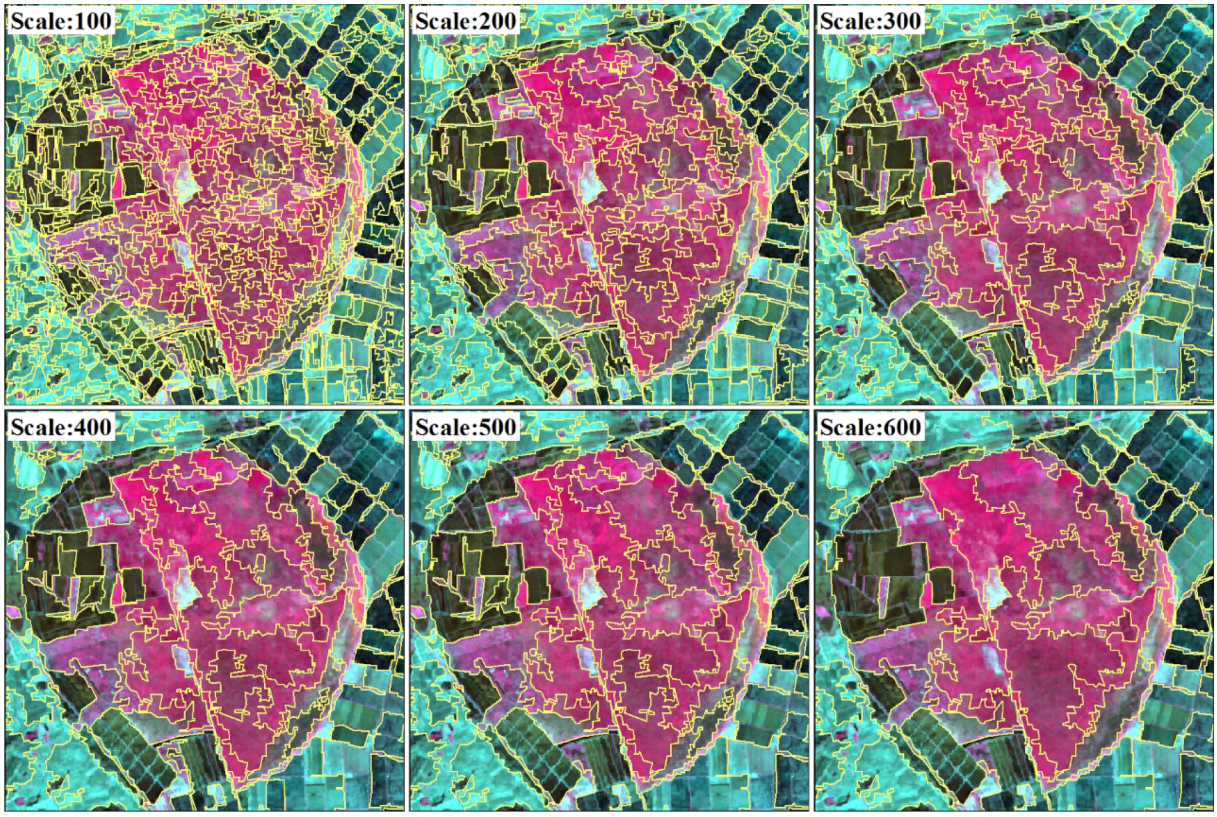

Fig. 4. Example for multi-resolution segmented results at different scales; the background image is Landsat OLI image (composited from bands 5, 4, 3) in Jun 1, 2015 (Path 114, Row 27) located in China's Sanjiang Plain.

wetlands and with normalized difference built-up index (NDBI) and bare surface index (BSI) to determine urban wetlands. Secondly, an initial threshold (0.05) of NDVI was used to separate vegetated and non-vegetated wetlands with normalized difference moisture index (NDMI) being used as an auxiliary index. Different NDVI thresholds referencing to the statistic results were tested for sub-regions to modify the results of those categories. Thirdly, phenology difference, texture, and NDVI were combined to separate paddy field from marsh and swamp. Brightness and modified normalized difference water index (mNDWI) were combined to separate waterbody from tidal flat and salt pan. Furthermore, patch shape and artificial footprint were mostly applied to classify different waterbodies, while brightness, texture, and NDVI were used jointly to delineate marsh and swamp. Although other classifiers such as Nearest Neighbor (NN) and SVM could be used in the classification process, the approach of hierarchical decision trees is suitable for the identification of diverse wetland categories.

In this study, China was divided into seven work areas (Fig. 2) based on terrain and climatic conditions. Fig. 6 presents an example of classification rules for delineating wetlands in a block of NEC. However, it's inappropriate to apply a static threshold to separate other land cover types from wetlands and diverse wetland categories in the entire country. Based on our priori knowledge, heterogeneous rule sets were designed, and various thresholds were tested for different task blocks. For examples, terrain conditions were adequately considered for plateau wetlands including the Qinghai-Tibet Plateau (QTP) and Yunnan-Guizhou Plateau (YGP), where mountain shadows could affect the lake delineation. Most of paddy fields are planted in eastern China, such as Northeast China (NEC), the lower and middle reaches of Yangtze River (YAR), and Southeast and South China (SSC). Therefore, in terms of the difference in vegetation phenology, marsh and paddy field were

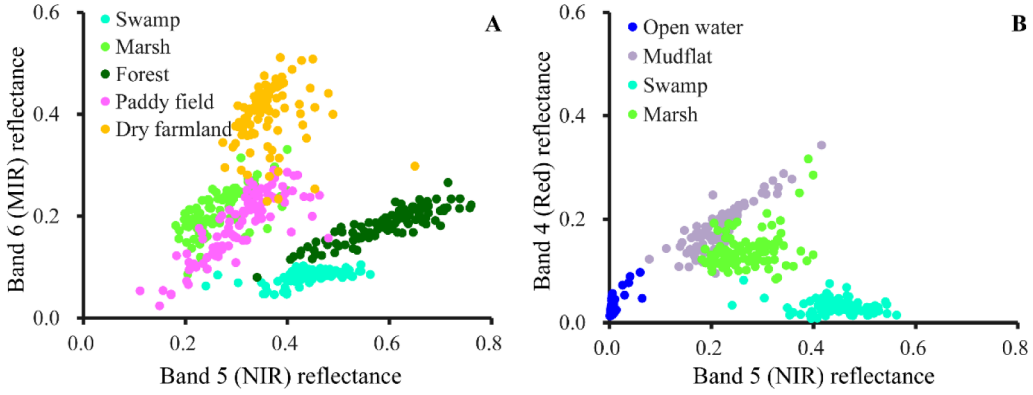

Fig. 5. Reflectance comparison between different Landsat 8 OLI image bands (mid-infrared, near-infrared, and red bands). A: for natural wetlands and other land cover types; B: for various wetland types.

Table 2
Feature list of image object identification for wetland classification.

Type	Feature Name	Parameters	Definition or description
Spectral features	Band reflectance	B1	Coastal band
		B7	Short-wave infrared 2
		Brightness	$(B_2 + B_3 + B_3 + B_5)/4$
	Spectral indices	NDWI	$((B_3 - B_5)/(B_3 + B_5)$
		NDMI	$(B_5 - -B_6)/(B_5 + B_6)$
		mNDWI	$(B_3 - -B_6)/(B_3 + B_6)$
		NDVI	$(B_5 - -B_4)/(B_5 + B_4)$
		RVI	B_5/B_4
		NDBI	$(B_6 - -B_5)/(B_6 + B_5)$
		NDSI	$(B_3 - -B_6)/(B_3 + B_6)$
		BSI	$(B_4 - -B_2)/(B_4 + B_2)$
Landscape features	Image color	Dark red color	Standard false color: vegetated wetland
		Blue color	Standard false color: waterbody
	Object texture	GLCM-contrast	Measures the local variations
		GLCM-entropy	A statistical measure of randomness
		Compactness	The degree to which an object is compact
	Patch shape	SI	Border length feature of image object divided by four times the square root of its area
		Length/width	Length-to-width ratio of an image object
	Phenology	Phenology information	Temporal difference
Environmental features	Topography	Elevation	DEM with a resolution 30 m
		Slope gradient	Generated from DEM
		Slope aspect	Generated from DEM
	Class relation	Neighbor distance	The distance of a class to another
		Object location	Geographic distribution

Note: B_{1-7} denote different bands of Landsat 8 OLI image; NDWI-normalized difference water index; NDMI-normalized difference moisture index; mNDWI-modified normalized difference water index; NDVI-normalized difference vegetation index; RVI-ratio vegetation index; NDBI-normalized difference built-up index; NDSI-normalized difference snow index; BSI-bare surface index; SI-shape index; GLCM-gray level co-occurrence matrix. All the parameters can be calculated in eCognition software (Version 9.2).

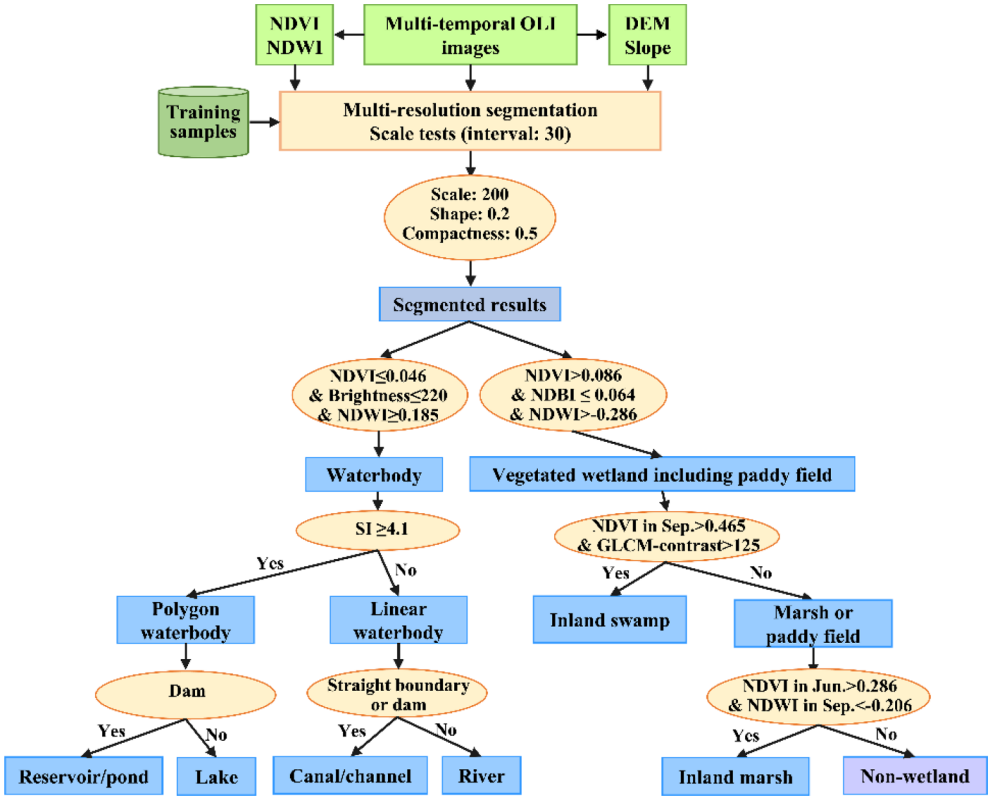

Fig. 6. an example of classification rules for delineating wetlands in a block of NEC.

separated from each other. While a single NDWI index or supervised classification is effective in extracting arid zone wetlands, e.g. the Inner Mongolia-Xinjiang Plateau (MXP), the spectral similarity of various wetland categories over the YAR and SSC requires multiple rules for an accurate separation. Moreover, human footprints were important for identifying reservoir/pond in the lower and middle reaches of Yellow River (YER) and YAR.

Delimitating the bilateral boundaries of coastal wetland is a critical

step to map China's wetlands. First, we worked on the coastline dataset published by Hou et al. (2016) based on Landsat images in 2015 and field samples along the coasts. Second, we extracted the first contour for a marine water depth of 6 m, which is the closest to coastline, from the global relief model (GRM) data acquired from the National Centers for Environmental Information of United States (https://www.ngdc.noaa.gov/) as the seaward boundary of coastal wetlands. Third, the landward 15 km-buffer line from coastline was determined to be the boundary between inland and coastal wetlands.

2.4.2. Post classification improvement

Due to the complexity of various wetland cover types, it is difficult to accurately discriminate the spectrally similar categories in some areas. With the accuracy of wetland mapping as the ultimate goal, correction for misclassification and inaccurate boundary delineation was carried out to revise the HOHC results after the first validation. The HOHC results were revised for four rounds assisted by extensive field data as well as data from other references till the best possible classification accuracy was achieved. The final wetland results were exported as vector data layers by the eCognition software. After standardizing the attribute table for each data layer, all the layers were merged together to generate the final wetland map. The resultant wetland layer and previous wetland datasets were compared by use of the ArcGIS software, and large differences between these products were manually checked with reference to the Landsat images to confirm our final classification.

2.4.3. Validation of mapping result and uncertainty analysis of wetland estimation

The classified results in different versions were assessed against the same field samples (5022) for each wetland category. A confusion matrix including the overall accuracy, producer and user's accuracies, and kappa coefficient was used to assess classification accuracy. The error margin at a confidence level of 95% was presented for the area of each wetland category.

2.5. Data analysis and integration

In this study, the distribution pattern and area of each wetland category were documented, and the spatial variability of wetlands was examined across different provinces or geographic regions, and in terms of precipitation gradient and elevation interval. The mapping and analyzed results were integrated to generate a new wetland dataset, so named CAS_Wetlands, i.e., wetland dataset of CAS, at 1: 100,000 scale. The CAS_Wetlands will be made publically available for related scientific studies and wetland management.

3. Results

3.1. Classification accuracy

The initial wetland mapping result by HOHC was validated by 5022 samples and had an overall accuracy of 80.6%. As shown in Table 3, however, the overall accuracy and kappa coefficient for the CAS_Wetlands were 95.1% and 0.94, respectively, after four rounds of manual editing. For the category I wetlands, each of the three wetland types was classified with producer's and user's accuracies over 96% and 94%, respectively. The producer's accuracy for the category II wetlands was over 90% and the user's accuracy was above 85%. Specifically, shallow marine water was classified at the highest accuracy, followed by tidal flat. Salt pan and reservoir/pond were classified at the lowest classification producer's accuracy to which the error from lake was a main contributor. In addition, the classification accuracy for inland swamp was low among the inland wetland categories, which was primarily attributed to its erroneous omission from inland marsh. Fig. 7 illustrates the typical wetland categories delineated.

Table 3
Classification accuracy of wetland categories for the CAS_Wetlands.

Category I	Category II	Sample number	Producer's accuracy	User's accuracy
Inland wetland	Inland swamp	97	91.8%	89.9%
	Inland marsh	1625	95.4%	98.1%
	Lake	430	95.1%	91.9%
	River	1177	96.5%	96.2%
	Total	3329	98.0%	98.7%
Coastal wetland	Coastal swamp	292	95.9%	97.2%
	Coastal marsh	209	95.7%	90.9%
	Lagoon	21	95.2%	100.0%
	Estuarine water	43	93.0%	85.1%
	Tidal flat	197	97.5%	99.5%
	Shallow marine water	92	97.8%	96.8%
	Total	854	98.7%	97.9%
Human-made wetland	Reservoir/pond	414	91.3%	89.4%
	Canal/channel	83	94.0%	87.6%
	Salt pan	133	90.2%	94.5%
	Aquaculture pond	209	93.3%	89.9%
	Total	839	96.3%	94.4%
Summary		5022	Overall = 95.1%	Kappa = 0.94

3.2. Area and distribution of China's wetlands

The area for each wetland category is summarized in Table 4. The wetland area in China was estimated to be 451,084 ± 2014 km^2 in 2015. As shown in Fig. 8, wetlands were extensively distributed across the country with a notable spatial heterogeneity.

Inland wetland was estimated to be 317,966 ± 899 km^2, accounting for 70.5% of the total wetland area in China. Inland marsh, as one of the most important inland wetlands, was the dominant wetland category with an area of 152,429 ± 373 km^2 accounting for 33.8% of the total wetlands, and was mostly observed in the NEC and QTP. As an important water resource, lake was primarily observed in the QTP, YAR, and NEC, while river was extensively found in the whole China. Inland swamp having the smallest inland wetland area (8230 ± 191 km^2) was mostly present in the northern NEC.

Human-made wetland had an area of 70,709 ± 634 km^2 in 2015 and was primarily identified in the eastern irrigation-agriculture areas of China. Reservoir/pond was the dominant human-made wetland category (72.8%), with an estimated area of 51,485 ± 293 km^2. Aquaculture pond was extensively observed over the coasts with an area of 11,896 ± 124 km^2, contributing to 16.8% of human-made wetlands. Other two human-made wetland categories, canal/channel and salt pan, were estimated to be 4621 ± 129 km^2 and 2707 ± 88 km^2, respectively.

Coastal wetland was widely delineated over the coastal zone while its area was estimated to be 62,409 ± 481 km^2, accounting for 13.8% of the whole wetlands. Among which, shallow marine water was the largest coastal wetland category (55,367 ± 373 km^2 or 88.7%) providing important habitats for marine organism. Coastal marsh had the second largest area (2979 ± 22 km^2) among coastal wetlands, followed by tidal flat (2375 ± 23 km^2). Estuarine water and lagoon were also important coastal wetland categories. Moreover, coastal swamp dominated by mangroves had an area of 259 ± 15 km^2 and played an important role in coastal protection.

3.3. Geospatial pattern of wetlands in China

For a better understanding of the spatial pattern of China's wetland distributions, the category I wetlands were extracted in terms of province, geographic region, precipitation gradient, and elevation interval

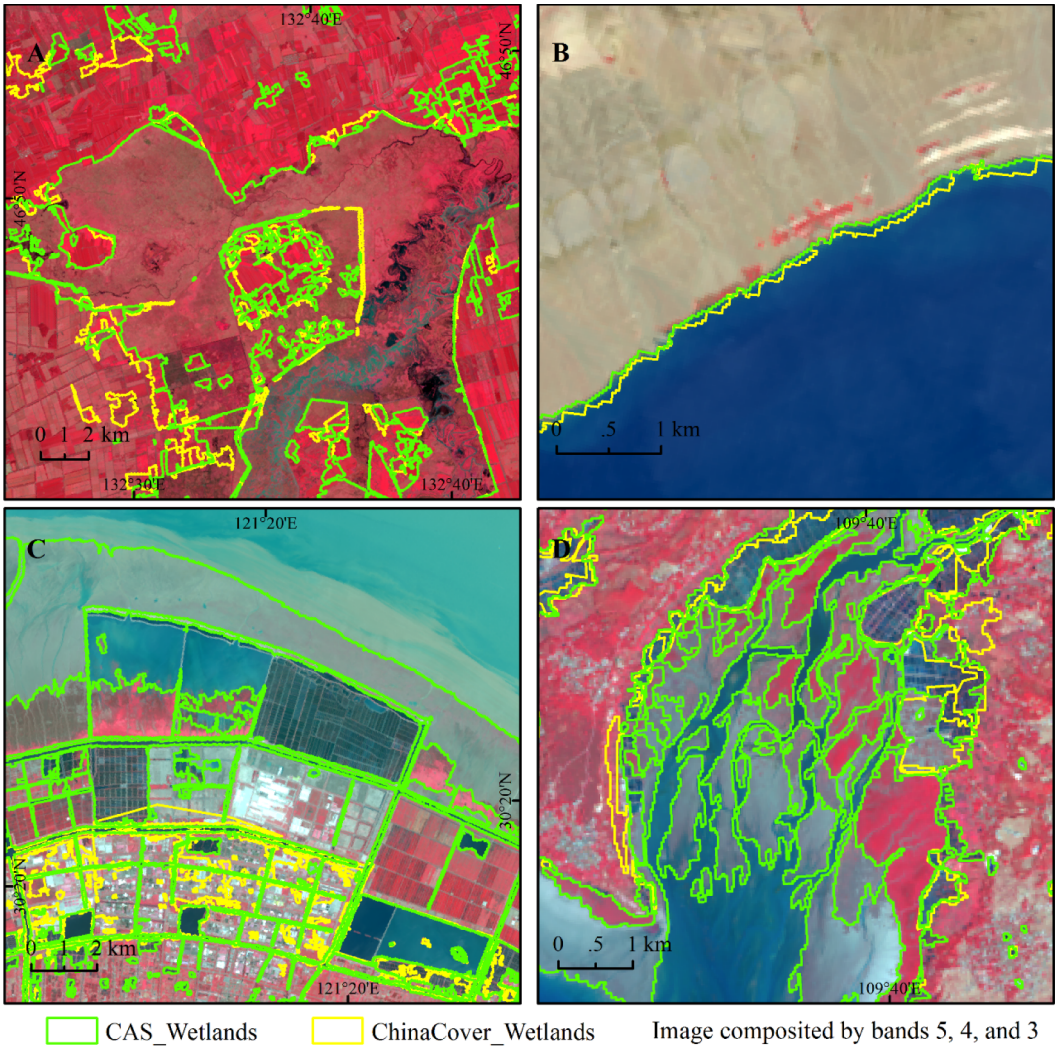

Fig. 7. Typical subsets of CAS_Wetlands at 30 m scale are compared with those in the ChinaCover dataset in 2010. A: marshes in Heilongjiang Province (Path 114/ Row 27); B: lakes in Tibet Autonomous Region (Path 139/ Row 38); C: coastal wetlands in Shanghai City (Path 118/ Row 39); and D: costal swamps in Guangxi Autonomous Region (Path 124/ Row 45).

Table 4
Area in various wetland categories in China.

Category I	Category II	Area (km^2)
Inland wetland	Inland swamp	8230 ± 191
	Inland marsh	152,429 ± 373
	Lake	83,821 ± 205
	River	73,486 ± 130
	Total	317,966 ± 899
Human-made wetland	Reservoir/pond	51,485 ± 293
	Canal/channel	4621 ± 129
	Salt pan	2707 ± 88
	Aquaculture pond	11,896 ± 124
	Total	70,709 ± 634
Coastal wetland	Coastal swamp	259 ± 15
	Coastal marsh	2979 ± 22
	Lagoon	316 ± 17
	Estuarine water	1113 ± 31
	Tidal flat	2375 ± 23
	Shallow marine water	55,367 ± 373
	Total	62,409 ± 481
Summary		451,084 ± 2,014

as illustrated in Fig. 9. The areal information is provided in the appendix Tables A1–4.

China's wetlands were mainly distributed in the northern inland regions (Fig. 9A), especially in Tibet, Qinghai, Inner Mongolia, Heilongjiang, and Xinjiang Provinces. The total wetland area in these five provinces accounted for 53.7% of the total wetland area in China. The same situation was found for inland wetlands. Coastal wetlands were mostly observed in Liaoning Province, followed by Guangdong and Zhejiang provinces, while human-made wetlands were primarily identified in Jiangsu and Guangdong provinces, where aquaculture ponds contributed most. Large area of human-made wetlands were also found in Hubei Province which could be explained by the dominant distribution of reservoirs, such as the Three Gorges Reservoir.

Geographic region is an important study scale for describing wetland research. We compared the areal variation of wetlands (Fig. 9B) and revealed that the QTP and NEC were the dominant regions of China's wetlands, where the wetland area accounted for 50% of the total China's wetlands, while the QTP had the largest wetland coverage (6%). Coastal wetlands were mostly observed in the YAR and SSC with long coastlines. Moreover, the YAR had the largest area of human-made

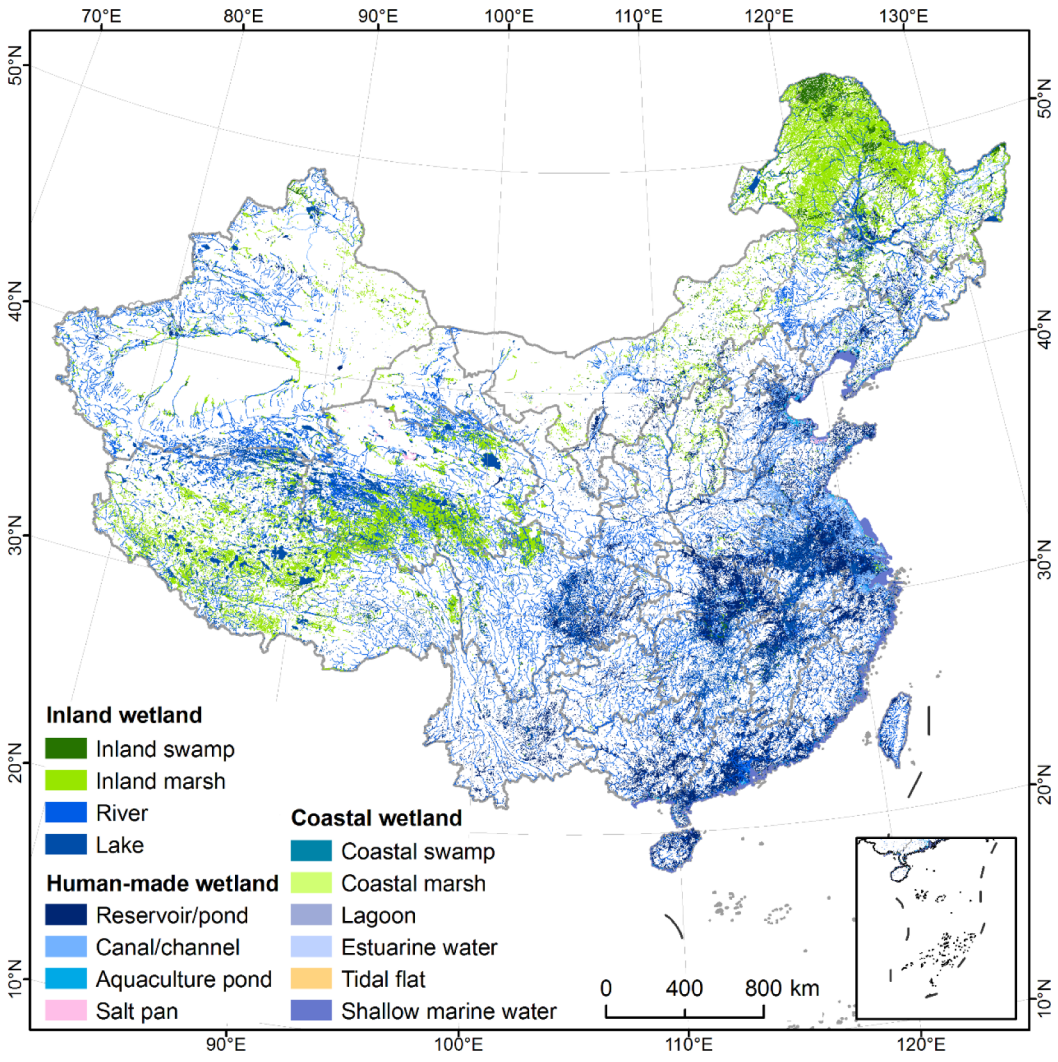

Fig. 8. Spatial distribution of wetlands in China by CAS_Wetlands.

wetland (26,104 km^2) due to its extensive distribution of both reservoirs in the plains and aquaculture ponds along the coasts.

Hydrological conditions are critical to the existence of wetlands, and thus precipitation is an important factor influencing the distribution of wetlands in China. As shown in Fig. 9C, the wetland area was examined in terms of the precipitation gradient. It was estimated that wetlands in China were dominantly (42.4%) observed in the regions with an annual precipitation level between 300 and 600 mm. Inland wetlands were mainly observed at an annual precipitation level of 300–600 mm and were the least at 1500 mm or above. Both coastal and human-made wetlands were mostly identified at annual precipitation levels of 1000–1500 mm, but limited in the regions with an annual precipitation lower than 300 mm.

Because elevation has an important effect on wetland formation, Fig. 9D shows a comparison of wetland areas over different elevation intervals. Interestingly, wetlands in China were primarily found in the regions with elevation lower than 200 m (42.8%) and higher than 3000 m (28.1%). Inland wetlands were mainly distributed in the region with elevation higher than 3000 m (39.8%), while coastal wetlands (99.9%) and human-made wetlands (78.0%) were mostly present at elevation less than 200 m. Few human-made wetlands were mapped in the regions with elevation larger than 3000 due to limited human activities.

4. Discussion

4.1. Landsat 8 OLI images and the HOHC

The quality and capacity of Landsat 8 OLI images have been improved than the previous Landsat sensors (Roy et al., 2014). Such improvement enables an accurate mapping of China's wetlands. As shown in Fig. 5, spectral differences of land cover types in red (band 4), near infrared (band 5) and short-wave infrared bands (band 6) allow to use NDVI, NDMI, and other indices to separate open water from vegetation and other lands, as well as marsh from swamp effectively. Time series Landsat 8 OLI images continued the advantages for mapping different wetland categories. In the NEC plains, wet season generally begins in May and ends in September. When paddy fields are still in the inundation stage in late May, marshes are in the leafing stage with a closed canopy (Dong et al., 2016). This phenological difference between marsh and paddy field was captured by time series OLI images for distinguishing marsh from paddy field (Fig. 10).

Because separation of wetland from other land cover types is usually easier than separation within wetland categories (Ozesmi and Bauer, 2002), the HOHC resulted in a good classification accuracy, and thus yielded an improved classification for China's wetlands. Compared with traditional visual interpretation, decision tree-based classification is

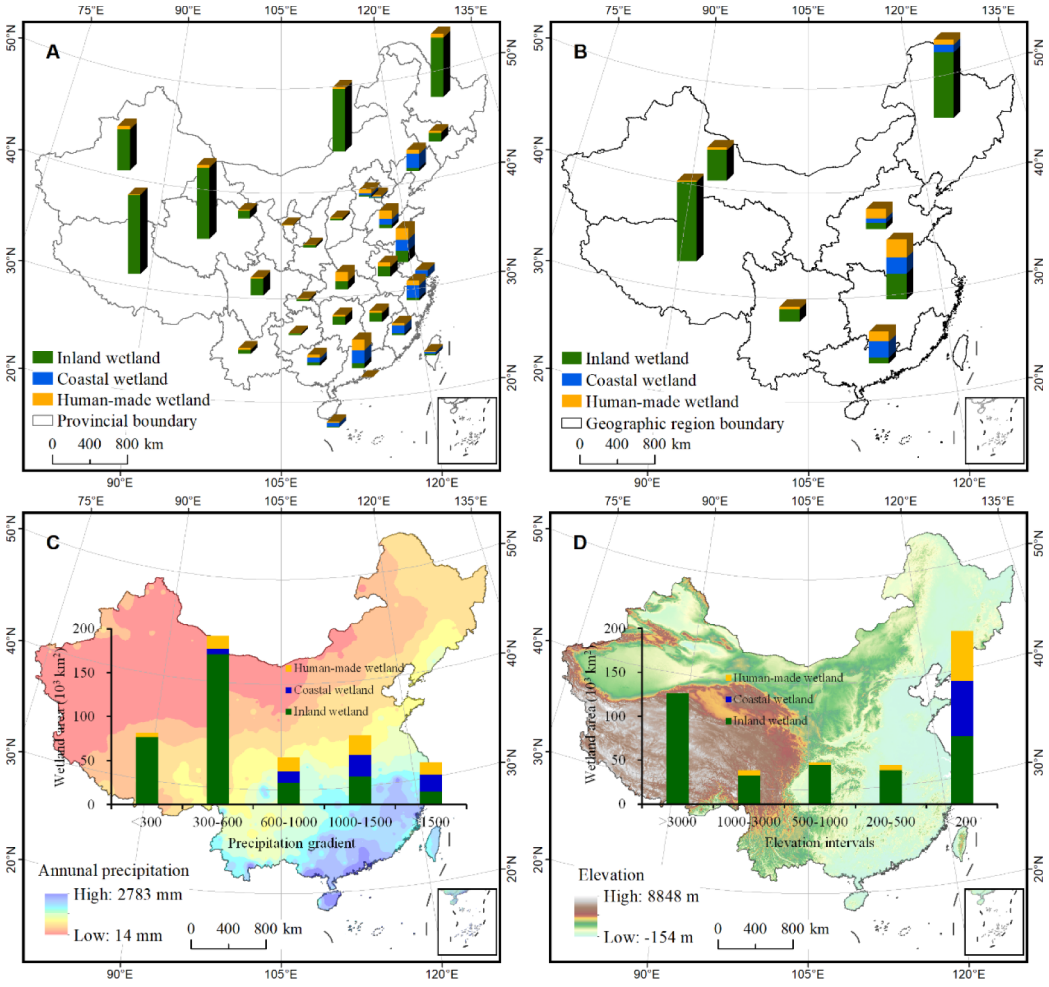

Fig. 9. Geospatial variations of wetland area in China: comparison at scale of provinces (A), geographic regions (B), precipitation gradients (C), and elevation intervals (D).

more acceptable for mapping wetlands at a broad scale due to the improved process efficiency (Zhang et al., 2014). A large number of studies applied diverse machine learning algorithms and different remote sensing data for a rapid wetland mapping (Amani et al., 2019b; Ludwig et al, 2019). However, the complexity of diverse wetland categories makes it difficult for an automated image classification to be optimal. The automated classifiers are mostly pixel-based and difficult to achieve a high classification accuracy for mapping wetlands at a broad scale due to limited and un-presentative training samples and difficulty in controlling the classification process (Lei et al., 2016; Mui et al., 2015). For example, separating different waterbodies including lake, river, reservoir/pond, estuarine water, lagoon, and shallow marine water is difficult using automated classification by training samples due to similar spectral and texture features. Therefore, another novelty of this study is the hybridization of the OBIA and hierarchical and spatially varying classification rules to achieve an accurate delineation of various wetland categories. This approach is semi-automated and controllable in different classification nodes of the classification process. As compared in Fig. 10, OBIA smoothened local noises at the object level, and effectively reduced the “salt and pepper” effect which would otherwise be introduced by pixel-based classification. As mountain shadow is an important error source for distinguishing waterbody (Zhang et al., 2019), topographic indices, such as slope derived from DEM data, were used for mapping alpine lakes on the TP. Generally, a single rule or index threshold could be applied to delineate a specific wetland category in neighborhood regions, but may not be effective in remote regions, implying that selecting optimal indices and their threshold values was critical for the delineation of a specific wetland category in different geographic regions. In this study, the division of geographic regions, i.e., seven work areas, and image-based task blocks play a vital role in establishing the rule sets and optimizing the thresholds for wetland classification.

This study has presented an improved wetland mapping approach and a data product in China (Fig. 8). The HOHC played a critical role in ensuring the accuracy of CAS_Wetlands. On the other hand, uncertainties exist in this dataset resulting from empirical settings segmentation parameters and classification thresholds in some task blocks, especially in the areas with limited field samples. For example, few field samples were available for inland swamp over the Greater Khingan Mountains area where the wetland landscape has complex boundaries due to terrain and climatic conditions. We thus have to use some empirical values in the segmentation and classification rules. Therefore, the determination of optimum parameters for segmentation deserves further investigations (Hossain and Chen, 2019).

4.2. CAS_Wetlands versus other wetland datasets

This study performed the most detailed national wetland mapping with remote sensing data at 30-m spatial resolution (CAS_Wetlands). First, the mapping results were built upon the Ramsar definition of wetland categories, which are most commonly used for sustainable ecosystem management and ecological research. The wetland classification system for remote sensing developed in this study was established based on the unprecedented field sample effort in the history of

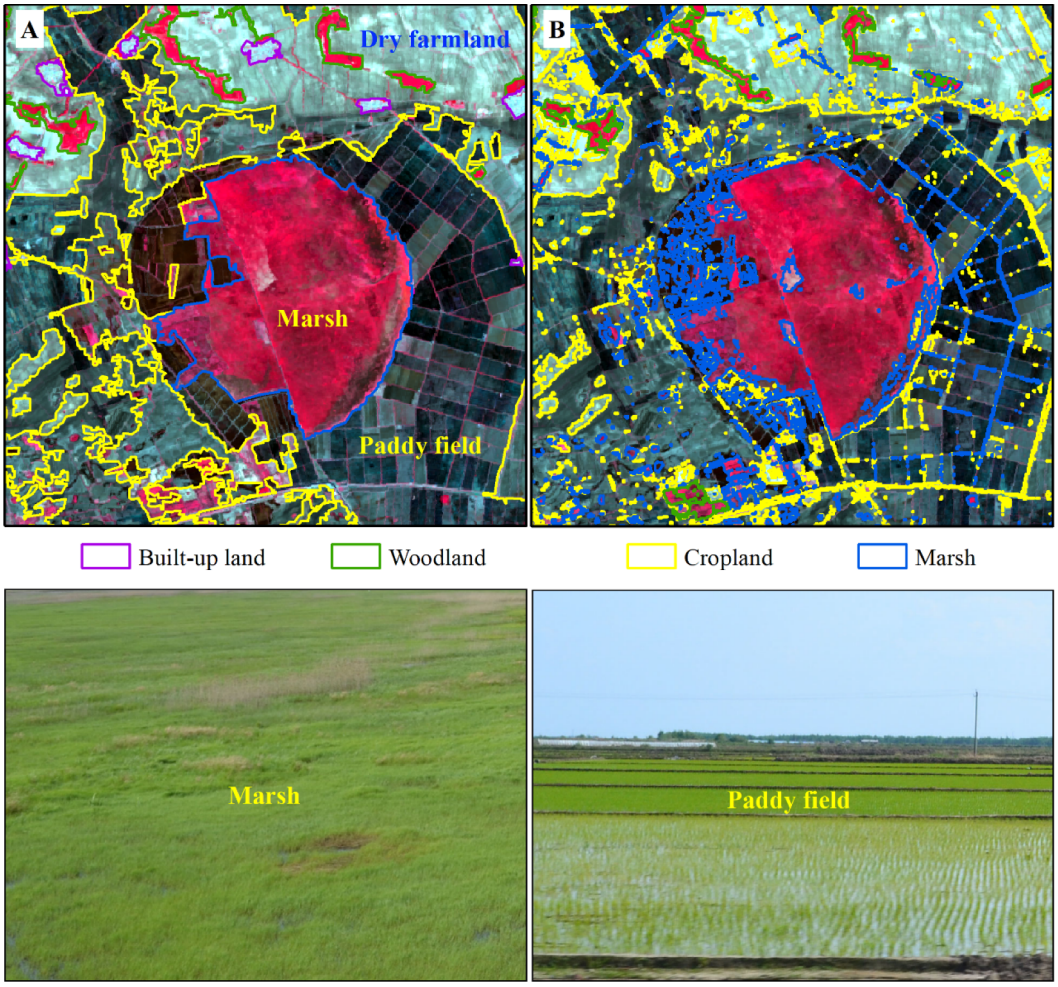

Fig. 10. Phenology-based differentiation of marsh from paddy field is obvious shown in Landsat OLI false color images (Path 114/ Row 27, in Jun 1, 2015) and by the classification with either between object-based (A) or pixel-based approaches (B); the corresponding photos were taken in early June 2015 over the Sanjiang Plain, Northeast China.

wetland mapping in the country, accommodating both ecological definitions and remote sensing image classification. Both the CLUD (Liu et al., 2014) and ChinaCover (Mao et al., 2018a) in China and other global land cover databases (Table 5), e.g. FROM-GLC (Gong et al., 2013) aimed at estimating the areas of land use or land cover types and revealing their patterns, and thus their classification systems did not include inland, human-made, and coastal wetlands. Three previous national wetland observations (Gong et al., 2010; Niu et al., 2009,

Table 5
Comparison between the estimated areas of wetlands by different studies.

Research or Report	Mapping method	Image date	Data-source and product resolution	Estimated wetland area (km^2)			
				Inland	Coastal	Human-made	Total
Niu et al., 2012	Visual interpretation	1978	Landsat MSS, 240 m	286,400	13,104	9793	309,297
		2008	CBERS CCD, 240 m	275,482	10,035	38,892	324,097
Niu et al., 2009	Visual interpretation	1999–2002	Landsat ETM+, 30 m	339,352	17,610	2786	359,478
Gong et al., 2010	Visual interpretation	1987–1992	Landsat TM	318,326	14,335	22,546	355,208
		1999–2002	Landsat ETM+	257,922	12,015	34,911	304,849
Ma et al., 2012	Synergistic approach	–	Census and spatially explicit datasets, 1000 m	–	–	–	384,864
Mao et al., 2018a (ChinaCover)	OBIA and visual interpretation	1990	Landsat TM, 30 m	–	–	–	359,799
		2000	Landsat TM and ETM+, 30 m	–	–	–	355,236
		2010	HJ-1 CCD, 30 m	–	–	–	357,118
Liu et al., 2014 (CLUD)	Visual interpretation	2000	Landsat TM, ETM+, 30 m	–	–	–	256,878
NWI reports	Field investigation	1995–2003	Field observation	302,588	59,417	22,850	384,855
	Field investigation and auxiliary visual interpretation	2009–2013	CBERS CCD, SPOT 5 RADARSAT, 20 m	410,608	57,959	67,459	536,026
Lehner and Döll, 2004 (GLWD)	Data aggregation	2000 s	Multiple data source	–	–	–	311,000
This study (CAS_Wetlands)	HOHC	2015	Landsat 8 OLI, 30 m	317,966	62,409	70,709	451,084

2012) and the NWIs (Table 5) did not separate marsh and swamp from each other though they are clearly different wetland categories with the former being dominated by herbaceous vegetation and the latter by woody vegetation. These issues have been addressed in the CAS_Wetlands. The CAS_Wetlands also includes a class category for shallow marine water at depth less than six meters with the GRM data. This new classification system, as the guiding principal of the research, established an authoritative example for continued efforts in wetland monitoring across the country in the future. In particular, it is directly replicable to Landsat-8 OLI data.

Early Landsat sensors (MSS, TM, ETM +) and CBERS had limitations in acquiring high-quality images of some areas. This may introduce the uncertainty in mapping national wetlands due to the fact that it may take several years to complete the workable images. Meanwhile, traditional visual interpretation is a preferred classification method, but can lose a lot of small wetlands. These two factors could contribute to an underestimation of China's wetlands (Gong et al., 2010; Niu et al., 2009, 2012). Another weakness of the mentioned observations is that ground reference samples were not used in the classification and field validation was not performed. Although the two NWIs combined field investigation with remote sensing classification, the estimated area of China's wetland has large uncertainty due to the errors from wetland recognition and inconsistent observations possibly induced by a large team that consisted of more than 20,000 technicians from more than 200 institutions. If so, the data upon which the proposed "red line" for the conservation of at least 800 million mu (53.33 million ha) of wetlands is based might need to be revised. Another two other studies (Lehner and Döll, 2004; Ma et al., 2012) produced a raster wetland map of China at a spatial resolution of 1 km with pre-existing data, but the coarse resolution and the classification systems failed to meet the country's need.

Besides the improved remote sensing data and classification method, abundant ground truth samples and several rounds of manual editing greatly improved the accuracy of our wetland mapping results. The overall accuracy for the initial wetland classification by HOHC is 80.6%. This is an acceptable accuracy for such a large scale mapping study. However, considering that this dataset and the quantified data will be shared with and used by peer scientists in regional studies, four rounds of manual editing was performed to improve the accuracy to 95.1% for wetlands. This accuracy improvement was made by referencing multi-source data such as google earth images and field samples. For example, corrections were made for some swamps misclassified from forest and marsh in the mountainous regions of the NEC and some marshes misclassified from grassland in the TP. Moreover, some inaccurate boundaries of segmented wetland objects were also corrected. The historical datasets such as lake and reservoir database and China's vegetated wetland map were important references. The field references included both the sites archived from two previous national surveys and the field observations of this study. These reference and validation samples (16,496 samples) assure the quality of wetland mapping using Landsat images. Zhang et al. (2019) reported that the total area of lakes larger than 1 km^2 in China was 74,395 km^2, and our result gives an area of 75,726 km^2 with 83,821 km^2 being the area of all the lakes. This agreement is originated from using many high-resolution images such as Chinese GF-2 images to identify artificial dams and subsequently differentiate reservoirs from lakes. We also notice that the human-made wetland area estimated in this study is slightly larger than the number by the second NWI (4.6%), which could be attributed to the recent expansion of aquaculture ponds (Ren et al., 2019).

4.3. Implications of fine wetland classification for biodiversity conservation and ecosystem management

This study resulted in a completely new national wetland map of China, i.e., CAS_Wetlands. We considered such a high accuracy wetland mapping product a remarkable novelty. Therefore, this up to date and most accurate product has many potential applications in scientific research and decision making towards wetland conservation and management practice in China and around the world. Besides the accurate area of total wetlands in China, this study classified wetlands into 3 broad categories and 14 sub-categories. Such fine wetland classification will markedly benefit China's biodiversity conservation and sustainable ecosystem management. In this study, coastal wetlands were classified into six categories. Tidal flats providing dominant foraging habitats for migratory birds experienced severe shrinkage due to human encroachment (Mao et al., 2018a) and exotic plant invasion (Mao et al., 2019b). Meanwhile, the accurate delineation of aquaculture ponds and salt pans can help understand the intensity of human utilization upon coastal zones and protecting coastal ecosystems. Moreover, there is clear difference in the ecological function and service between swamp and marsh, such as carbon sequestration ability (Rocha and Goulden, 2009). We separated these two vegetated wetland categories and thus speculated that the reported studies, such as Xiao et al. (2018), overestimated the China's wetland carbon storage and marshland CH_4 release due to the overestimation of marsh area and limited wetland categories (Wei et al., 2019). Different with the five categories, i.e., *coastal wetland, lake, river, vegetated wetland, and human-made wetland*, in the NWIs, this new wetland observation demonstrated the feasibility of the proposed wetland classification system for remote sensing, and accurately determined the area of diverse wetland categories that can benefit estimation of wetland carbon storage and greenhouse gas emission.

Although CAS_Wetlands results from the delineation of 14 sub-categories at the landscape scale using moderate resolution satellite images, finer wetland classification is still necessary for wetland conservation and management. For example, *Bolboschoenus planiculmis,* a wetland plant, is an important food source for migratory waterfowls, such as endangered *Siberian cranes*, and thus examining their distribution is critical to biodiversity conservation and protected area management. *Spartina Alterniflora*, the most rampant invasive plant species in coastal wetlands of China, needs to be accurately monitored to protect native species and ensure ecological security (Mao et al., 2019b). Since the plant functional traits play critical roles in ecosystem process, an effective wetland ecosystem conservation and management plan requires further investigation on plant functional groups (Rebelo et al., 2018). Such investigation calls for hyperspectral and high spatial resolution images acquired by different remote sensing platforms, e.g. unmanned aerial vehicle, and new image classification methods (Amani et al., 2018; Ludwig et al., 2019). Considering China's huge population, rapid urbanization and economic development, as well as notable climate change, a scientific conservation system combining site specific protection approaches with effective remote sensing observation are necessary for sustainable wetland ecosystems (Xu et al., 2019).

5. Conclusions

National wetland mapping in China is achieved in this study by applying the HOHC and a new designed wetland classification system to Landsat 8 OLI images. This study has resulted in the most accurate up-to-date estimation for various wetlands of China. The wetland area is estimated to be 451,084 ± 2014 km^2, of which 70.5% are inland wetlands. Of the 14 wetland categories, inland marsh has an area of 152,429 ± 373 km^2, which is 33.8% of the whole wetlands and mostly observed in the NEC and QTP. The distribution of wetland category varies among provinces, geographic regions, precipitation gradients, and elevation intervals. Considering the sustainable conservation and management, wetland classification for differentiation of plant species or functional groups by means of multi-source remote sensing data is still necessary for China.

Declaration of Competing Interest

The authors declare that they have no known competing financial interests or personal relationships that could have appeared to influence the work reported in this paper.

Acknowledgements

This study was jointly supported by the National Key Research and Development Program of China (2016YFA0602301, 2016YFC0500201, and 2016YFC0500408), the National Natural Science Foundation of China (41771383, 41671219, and 41730643), the outstanding Young Scientist Foundation of IGA, CAS (Y5H1061001), the funding from Youth Innovation Promotion Association of Chinese Academy of Sciences (2017277, 2012178), and the National Earth System Science Data Center (http:// www.geodata.cn). We are very grateful to those who participated in the image classification and field investigation for mapping China's wetlands. We thank Prof. Bingfang Wu for providing field wetland samples and Prof. Xiyong Hou for providing China's coastline dataset. We appreciate the facility that make Landsat 8 OLI images accessible through the USGS and the satellite and geospatial data provided by the ISDP. We also thank the three anonymous reviewers for the constructive comments and suggestions, which help improve the quality of this manuscript.

Appendix A. Supplementary data

Supplementary data to this article can be found online at https://doi.org/10.1016/j.isprsjprs.2020.03.020.

References

Adam, E., Mutanga, O., Rugege, D., 2010. Multispectral and hyperspectral remote sensing for identification and mapping of wetland vegetation: a review. Wetl. Ecol. Manage. 18 (3), 281–296.

Amani, M., Salehi, B., Mahdavi, S., Brisco, B., 2018. Spectral analysis of wetlands using multi-source optical satellite imagery. ISPRS J. Photogramm. Remote Sen. 114, 119–136.

Amani, M., Brisco, B., Afshar, M., Mirmazloumi, S.M., Mahdavi, S., Mirzadeh, S.M.J., Huang, W., Granger, J., 2019a. A generalized supervised classification scheme to produce provincial wetland inventory maps: an application of Google Earth Engine for big geo data processing. Big Earth Data 3 (4), 378–394.

Amani, M., Mahdavi, S., Afshar, M., Brisco, B., Huang, W., Mirzadeh, S.M.J., White, L., Banks, S., Montgomery, J., Hopkinson, C., 2019b. Canadian wetland inventory using Google Earth Engine: the first map and preliminary results. Remote Sens. 11, 842. https://doi.org/10.3390/rs11070842.

Asselen, S., Verburg, P.H., Vermaat, J.E., Janse, J.H., 2013. Drivers of wetland conversion: a global meta-analysis. PLoS One 8, 381292. https://doi.org/10.1371/journal.pone.0081292.

Blaschke, T., 2010. Object based image analysis for remote sensing. ISPRS J. Photogramm. Remote Sen. 65, 2–16.

Campbell, A., Wang, Y., 2018. Examining the influence of tidal stage on salt marsh mapping using high-spatial resolution satellite remote sensing and topobathymetric LiDAR. IEEE Trans. Geosci. Remote Sens. 56 (9), 5169–5176.

Campbell, A., Wang, Y., 2019. High spatial resolution remote sensing for salt marsh mapping and change analysis at Fire Island National Seashore. Remote Sens. 11 (9), 1107. https://doi.org/10.3390/rs11091107.

Campbell, A.D., Wang, Y., 2020. Salt marsh monitoring along the mid-Atlantic coast by Google Earth Engine enabled time series. PLoS ONE 15 (2), e0229605. https://doi.org/10.1371/journal.pone.0229605.

Cissell, J.R., Delgado, A.M., Sweetman, B.M., Steinberg, M.K., 2018. Monitoring mangrove forest dynamics in Campeche, Mexico, using Landsat satellite data. Remote Sens. Appl.: Soc. Environ. 9, 60–68.

Dong, J., Xiao, X., Menarguez, M.A., Zhang, G., Qin, Y., Thau, D., Biradar, C., Moore, B., 2016. Mapping paddy rice planting area in northeastern Asia with Landsat 8 images, phenology-based algorithm and Google Earth Engine. Remote Sens. Environ. 185, 142–154.

Dronova, I., Gong, P., Wang, L., 2011. Object-based analysis and change detection of major wetland cover types and their classification uncertainty during the low water period at Poyang Lake, China. Remote Sens. Environ. 115, 3220–3236.

Dronova, I., 2015. Object-based images analysis in wetland research: a review. Remote Sens. 7, 6380–6413.

Gallant, A.L., 2015. The challenges of remote monitoring of wetlands. Remote Sens. 7 (8), 10938–10950.

Gong, P., Niu, Z., Cheng, X., Zhao, K., Zhou, D., Guo, J., Liang, L., Wang, X., Li, D., Huang, H., Wang, Y., Wang, K., Li, W., Wang, X., Ying, Q., Yang, Z., Ye, Y., Li, Z., Zhuang, D., Chi, Y., Zhou, H., Yan, J., 2010. China's wetland change (1990–2000) determined by remote sensing. Sci. China-Earth Sci. 53, 1036–1042.

Gong, P., Wang, J., Yu, L., Zhao, Y., Zhao, Y., Liang, L., Niu, Z., Huang, X., Fu, H., Liu, S., Li, C., Li, X., Fu, W., Liu, C., Xu, Y., Wang, X., Cheng, Q., Hu, L., Yao, W., Zhang, H., Zhu, P., Zhao, Z., Zhang, H., Zheng, Y., Li, L., Zhang, Y., Chen, H., Yan, A., Guo, J., Yu, L., Wang, L., Liu, X., Shi, T., Zhu, M., Chen, Y., Yang, G., Tang, P., Xu, B., Giri, C., Clinton, N., Zhu, Z., Chen, J., Chen, J., 2013. Finer resolution observation and monitoring of global land cover: first mapping results with Landsat TM and ETM+ data. Int. J. Remote Sens. 34, 2607–2654.

Guo, M., Li, J., Sheng, C., Xu, J., Wu, L., 2017. A review of wetland remote sensing. Sensors 17, 777. https://doi.org/10.3390/s17040777.

Hossain, M.D., Chen, D., 2019. Segmentation for object-based image analysis (OBIA): A review of algorithms and challenges from remote sensing perspective. ISPRS J. Photogramm. Remote Sen. 150, 115–134.

Hou, X., Wu, T., Hou, W., Chen, Q., Wang, Y., Yu, L., 2016. Characteristics of coastline changes in mainland China since the early 1940s. Sci. China-Earth Sci. 59, 1791–1802.

Jia, M., Wang, Z., Zhang, Y., Mao, D., Wang, C., 2018. Monitoring loss and recovery of mangrove forests during 42 years: the achievements of mangrove conservation in China. Int. J. Appl. Earth Obs. Geoinf. 73, 535–545.

Kirwan, M., Megonigal, P., 2013. Tidal wetland stability in the face of human impacts and sea-level rise. Nature 504, 53–60.

Kloiber, S.M., Macleod, R.D., Smith, A.J., Knight, J.F., Huberty, B.J., 2015. A semi-automated, multi-source data fusion update of a wetland inventory for East-Central Minnesota, USA. Wetlands 35, 335–348.

Lehner, B., Döll, P., 2004. Development and validation of a global database of lakes, reservoirs and wetlands. J. Hydrol. 296, 1–22.

Lei, G., Li, A., Bian, J., Zhang, Z., Jin, H., Nan, X., Zhao, W., Wang, J., Cao, X., Tan, J., Liu, Q., Yu, H., Yang, G., Feng, W., 2016. Land cover mapping in southwestern China using the HC-MMK approach. Remote Sens. 8, 305. https://doi.org/10.3390/rs8040305.

Liu, J., Kuang, W., Zhang, Z., Xu, X., Qin, Y., Ning, J., Zhou, W., Zhang, S., Li, R., Yan, C., Wu, S., Shi, X., Jiang, N., Yu, D., Pan, X., Chi, W., 2014. Spatiotemporal characteristics, patterns, and causes of land-use changes in China since the late 1980s. J. Geogr. Sci. 24 (2), 195–210.

Liu, M., Mao, D., Wang, Z., Li, L., Man, W., Jia, M., Ren, C., Zhang, Y., 2018. Rapid invasion of *Spartina alterniflora* in the coastal zone of mainland China: new observations from Landsat OLI images. Remote Sens. 10, 1933. https://doi.org/10.3390/rs10121933.

Ludwig, C., Walli, A., Schleicher, C., Weichselbaum, J., Riffler, M., 2019. A highly automated algorithm for wetland detection using multi-temporal optical satellite data. Remote Sens. Environ. 274, 333–351.

MA (Assessment, Millennium Ecosystem), 2005. Ecosystems and human well-being: wetlands and water. World Resources Institute, Washington, DC, pp. 5.

Ma, K., You, L., Liu, J., Zhang, M., 2012. A synergistic approach using census and spatially explicit datasets. PLoS One 7, e47814.

Ma, R., Yang, G., Duan, H., Jiang, J., Wang, S., Feng, X., Li, A., Kong, F., Xue, B., Wu, J., Li, S., 2011. China's lakes at present: number, area and spatial distribution. Sci. China-Earth Sci. 54 (2), 283–289.

Mahdavi, S., Salehi, B., Granger, J., Amani, M., Brisco, B., Huang, W., 2017. Remote sensing for wetland classification: a comprehensive review. GISci. Remote Sens. 55 (5), 623–658.

Mao, D., Wang, Z., Wu, J., Wu, B., Zeng, Y., Song, K., Yi, K., Luo, L., 2018a. China's wetlands loss to urban expansion. Land Degrad. Dev. 29, 2644–2657.

Mao, D., Luo, L., Wang, Z., Wilson, M.C., Zeng, Y., Wu, B., Wu, J., 2018b. Conversions between natural wetlands and farmland in China: a multiscale geographical analysis. Sci. Total Environ. 634, 550–560.

Mao, D., Wang, Z., Yang, H., Li, H., Thompson, J.R., Li, L., Song, K., Chen, B., Gao, H., Wu, J., 2018c. Impacts of climate change on Tibetan lakes: patterns and processes. Remote Sens. 10, 358. https://doi.org/10.3390/rs10030358.

Mao, D., He, C., Wang, Z., Tian, Y., Xiang, H., Yu, H., Man, W., Jia, M., Ren, C., Zheng, H., 2019a. Diverse policies leading to contrasting impacts on land cover and ecosystem services in Northeast China. J. Clean. Prod. 240. https://doi.org/10.1016/j.jclepro.2019.117961.

Mao, D., Liu, M., Wang, Z., Li, L., Man, W., Jia, M., Zhang, Y., 2019b. Rapid invasion of Spartina alterniflora in the coastal zone of mainland China: spatiotemporal patterns and human prevention. Sensors 19, 2308. https://doi.org/10.3390/s19102308.

Möller, M., Lymburner, L., Volk, M., 2007. The comparison index: a tool for assessing the accuracy of image segmentation. Int. J. Appl. Earth Obs. Geoinf. 9 (3), 311–321.

Mui, A., He, Y., Weng, Q., 2015. An object-based approach to delineate wetlands across landscapes of varied disturbance with high spatial resolution satellite imagery. ISPRS J. Photogramm. Remote Sen. 109, 30–46.

Nahlik, A.M., Fennessy, M.S., 2016. Carbon storage in US wetlands. Nat. Commun. 7, 13835.

Niu, Z., Gong, P., Cheng, X., Guo, J., Wang, L., Huang, H., Shen, S., Wu, Y., Wang, X., Wang, X., Ying, Q., Liang, L., Zhang, L., Wang, L., Yao, Q., Yang, Z., Guo, Z., Dai, Y., 2009. Geographical characteristics of China's wetlands derived from remotely sensed data. Sci. China-Earth Sci. 52 (6), 723–738.

Niu, Z., Zhang, H., Wang, X., Yao, W., Zhou, D., Zhao, K., Zhao, H., Li, N., Huang, H., Li, C., Yang, J., Liu, C., Liu, S., Wang, L., Li, Zhan, Yang, Z., Qiao, F., Zheng, Y., Chen, Y., Sheng, Y., Gao, X., Zhu, W., Wang, W., Wang, H., Weng, Y., Zhuang, D., Liu, J., Luo, Z., Cheng, X., Guo, Z., Gong, P., 2012. Mapping wetland changes in China between 1978 and 2008. Chin. Sci. Bull. 57, 2813–2823.

Ozesmi, S.L., Bauer, M.E., 2002. Satellite remote sensing of wetlands. Wetl. Ecol. Manage. 10, 381–402.

Pekel, J., Cottam, A., Gorelick, N., Belward, A.S., 2016. High-resolution mapping of global surface water and its long-term changes. Nature 540, 418–422.
Prasad, K.A., Ottinger, M., Wei, C., Leinenkugel, P., 2019. Assessment of coastal aquaculture for India from sentinel SAR time series. Remote Sens. 11 (3), 357. https://doi.org/10.3390/rs11030357.
Rapinel, S., Fabre, E., Dufour, S., Arvor, D., Mony, C., Hubert-Moy, L., 2019. Mapping potential, existing and efficient wetlands using free remote sensing data. J. Environ. Manage. 247, 829–839.
Rebelo, A.J., Somers, B., Esler, K.J., Meire, P., 2018. Can wetland plant functional groups be spectrally discriminated? Remote Sens. Environ. 201, 25–34.
Ren, C., Wang, Z., Zhang, Y., Zhang, B., Chen, L., Xi, Y., Xiao, X., Doughty, R.B., Liu, M., Jia, M., Mao, D., Song, K., 2019. Rapid expansion of coastal aquaculture ponds in China from Landsat observations during 1984–2016. Int. J. Appl. Earth Obs. Geoinf. 82, 10192. https://doi.org/10.1016/j.jag.2019.101902.
Rezaee, M., Mahdianpari, M., Zhang, Y., Salehi, B., 2018. Deep convolutional neural network for complex wetland classification using optical remote sensing imagery. IEEE J.-STARS 11 (9), 3030–3039.
Rocha, A., Goulden, M.L., 2009. Why is marsh productivity so high? New insights from eddy covariance and biomass measurements in a *Typha* marsh. Agric. For. Meteorol. 149, 159–168.
Roy, D.P., Wulder, M.A., Loveland, T.R., Woodcock, C.E., Allen, R.G., Anderson, M.C., Helder, D., Irons, J.R., Johnson, D.M., Kennedy, R., Scambos, T.A., Schaaf, C.B., Schott, J.R., Sheng, Y., Vermote, E.F., Belward, A.S., Bindschadler, R., Cohen, W.B., Gao, F., Hipple, J.D., Hostert, P., Huntington, J., Justice, C.O., Kilic, A., Kovalskyy, V., Lee, Z.P., Lymburner, L., Masek, J.G., McCorkel, J., Shuai, Y., Trezza, R., Vogelmann, J., Wynne, R.H., Zhu, Z., 2014. Landsat-8: science and product vision for terrestrial global change research. Remote Sens. Environ. 145, 154–172.
Sheng, Y., Song, C., Wang, J., Lyons, E.A., Knox, B.R., Cox, J.S., Gao, F., 2016. Representative lake water extent mapping at continental scales using multi-temporal Landsat-8 imagery. Remote Sens. Environ. 185, 129–141.
Song, K., Wen, Z., Shang, Y., Yang, H., Lv, L., Liu, G., Fang, C., Du, J., Zhao, Y., 2018. Quantification of dissolved organic carbon (DOC) storage in lakes and reservoirs of mainland China. J. Environ. Manage. 217, 391–402.
Wang, Z., Wu, J., Madden, M., Mao, D., 2012. China's wetlands: conservation plans and policy impacts. AMBIO 41, 782–786.
Wang, X., Xiao, X., Zou, Z., Chen, B., Ma, J., Dong, J., Doughty, R.B., Zhong, Q., Qin, Y., Dai, S., Li, X., Zhao, B., Li, B., 2020. Tracking annual changes of coastal tidal flats in China during 1986–2016 through analyses of Landsat images with Google Earth Engine. Remote Sens. Environ. 238, 110987. https://doi.org/10.1016/j.rse.2018.11.030.
Wei, D., Li, T., Wang, X., 2019. Overestimation of China's marshland CH4 release. Glob. Change Biol. 25, 2515–2517.
Wohlfart, C., Winkler, K., Wendleder, A., Roth, A., 2018. TerraSAR-X and wetlands: a review. Remote Sens. 10, 916. https://doi.org/10.3390/rs10060916.
Xiao, D., Deng, L., Kim, D.G., Huang, C., Tian, K., 2018. Carbon budgets of wetland ecosystems in China. Glob. Change Biol. 25, 2061–2076.
Xu, W., Fan, X., Ma, J., Pimm, S.L., Kong, L., Zeng, Y., Li, X., Xiao, Y., Zheng, H., Liu, J., Wu, B., An, L., Zhang, L., Wang, X., Ouyang, Z., 2019. Hidden loss of wetlands in China. Curr. Biol. 29 (18), 3065–3071.
Yan, F., Liu, X., Chen, J., Yu, L., Yang, C., Chang, L., Yang, J., Zhang, S., 2017. China's wetland databases based on remote sensing technology. Chin. Geogr. Sci. 27, 374–388.
Zhang, L., Li, X., Yuan, Q., Liu, Y., 2014. Object-based approach to national land cover mapping using HJ satellite imagery. J. Appl. Remote Sens. 8, 083686. https://doi.org/10.1117/1.JRS.8.083686.
Zhang, G., Yao, T., Chen, W., Zheng, G., Shum, C.K., Yang, K., Piao, S., Sheng, Y., Yi, S., Li, J., O'Reilly, C.M., Qi, S., Shen, S.S.P., Zhang, H., Jia, Y., 2019. Regional differences of lake evolution across China during 1960s–2015 and its natural and anthropogenic causes. Remote Sens. Environ. 221, 386–404.
Zhu, P., Gong, P., 2014. Suitability mapping of global wetland areas and validation with remotely sensed data. Sci. China-Earth Sci. 57 (10), 2283–2292.
Zhu, Q., Peng, C., Chen, H., Fang, X., Liu, J., Jiang, H., Yang, Y., Yang, G., 2015. Estimating global natural wetland methane emissions using process modelling: spatio-temporal patterns and contributions to atmospheric methane fluctuations. Glob. Ecol. Biogeogr. 24, 959–972.